

Evaluation of the Re-entry Vulnerability Index to Predict Ventricular Tachycardia Circuits Using High Density Contact Mapping

Michele Orini PhD^{1,2}, Adam J. Graham MD³, Neil T. Srinivasan MD PhD³, Fernando O. Campos PhD⁴,
Ben M. Hanson PhD⁵, Anthony Chow MD FRCP³, Ross J. Hunter MD³, Richard J. Schilling MD FRCP³,
Malcolm Finlay MD PhD^{1,3}, Mark J. Earley MD FRCP³, Simon Sporton MD FRCP³, Mehul Dhinoja MD³,
Martin Lowe MD FRCP³, Bradley Porter MD⁶, Nicholas Child MD⁶, Christopher A. Rinaldi MD FRCP⁶,
Jaswinder Gill MD FRCP⁶, Martin Bishop PhD⁴, Peter Taggart MD DSci¹, Pier D. Lambiase MD FHRS^{1,3}

1: Institute of Cardiovascular Science, University College London, London, United Kingdom

2: The William Harvey Research Institute, Queen Mary University of London, London, United Kingdom

3: Electrophysiology Department, Barts Heart Centre, St Bartholomew's Hospital, London, United Kingdom

4: School of Biomedical Engineering and Imaging Sciences, King's College London, London, United Kingdom

5: Department of Mechanical Engineering, University College London, London, United Kingdom

6: Department of Cardiology, Guys and St Thomas' NHS Trust, London, United Kingdom

Address for correspondence:

- Professor Pier Lambiase, ICS UCL and Barts Heart Centre, London, UK: p.lambiase@ucl.ac.uk
- Dr Michele Orini, ICS UCL, London, UK : m.orini@ucl.ac.uk

Conflict of interest: none declared

Word count: 5000

Running title: RVI predicts VT exit sites during pacing

22 **Abstract**

23 **Background:** Identifying arrhythmogenic sites to improve ventricular tachycardia (VT) ablation
24 outcomes remains unresolved. The re-entry vulnerability index (RVI) combines activation and
25 repolarization timings to identify sites critical for re-entrant arrhythmia initiation without inducing VT.

26 **Objective:** To provide the first assessment of RVI's capability to identify VT sites of origin using high-
27 density contact mapping and comparison with other activation-repolarization markers of functional
28 substrate.

29 **Methods:** 18 VT ablation patients (16M, 72% ischemic) were studied. Unipolar electrograms were
30 recorded during ventricular pacing and analysed off-line. Activation time (AT), activation-recovery
31 interval (ARI), repolarization time (RT) were measured. Vulnerability to re-entry was mapped based
32 on RVI and spatial distribution of AT, ARI and RT. The distance from sites identified as vulnerable to
33 re-entry to the VT site of origin was measured, with distances <10 mm and >20 mm indicating accurate
34 and inaccurate localization, respectively.

35 **Results:** The origin of 18 VTs was identified (n=6 entrainment, n=12 pace-mapping). RVI maps included
36 1012, 408—2098 (median, 1st—3rd quartiles) points/patient. RVI accurately localized 72.2% VT sites of
37 origin, with median distance equal to 5.1, 3.2—10.1 mm. Inaccurate localization was significantly less
38 frequent for RVI than AT (5.6% vs 33.3%, OR=0.12, P=0.035). Compared to RVI, distance to VT sites of
39 origin was significantly larger for sites showing prolonged RT and ARI, and non-significantly larger for
40 sites showing highest AT and ARI gradients.

41 **Conclusion:** RVI identifies vulnerable regions closest to VT sites of origin. Activation-repolarization
42 metrics may improve VT substrate delineation and inform novel ablation strategies.

43

44 **Keywords:** Re-entry vulnerability index, activation time, repolarization time, ventricular tachycardia,
45 ablation, substrate mapping.

46 **Introduction**

47 Recurrence rates of ventricular tachycardia (VT) in structural heart disease remain sub-optimal at 50%
48 on average for a first time catheter ablation highlighting the need for more effective ablation
49 strategies ¹. Although VT induction and activation/entrainment mapping is the preferred method to
50 identify the circuit, this often cannot be performed due to instability of the VT itself or haemodynamic
51 compromise ². Substrate ablation strategies have been proposed and are based upon electrogram
52 features related to signal morphology or local conduction parameters ^{3,4}.

53 Despite the fact that the earliest research in the field identified spatio-temporal repolarization
54 dynamics as one of the fundamental factors modulating vulnerability to re-entry ⁵, current clinical
55 practice relies almost exclusively on conduction-related parameters to identify target sites. A
56 prerequisite for re-entry is unidirectional block whereby an activation wavefront blocks at a region of
57 late repolarization where tissue is still refractory, circumvents the area of block through slow
58 conducting pathways and re-enters the proximal region. The ability to re-enter the proximal region
59 depends not only on the conduction delay around the blocked area but also on the timing of the
60 returning wavefront relative to completion of repolarization and hence re-excitability in the proximal
61 region ⁶. This is the basis of the re-entry vulnerability index (RVI)^{6,7}, an activation-repolarization metric
62 that provides a point-by-point quantification of the likelihood of re-entry and enables functional VT
63 substrate delineation.

64 Previous mechanistic studies ⁶⁻⁹ based on ex-vivo animal data and computational models have
65 confirmed the link between RVI and sites of VT initiation. Preliminary observations on retrospective
66 data utilising non-contact mapping technology in selective RV disorders have shown encouraging
67 results ¹⁰. However, RVI's potential as a clinical tool to localize critical sites for VT initiation has never
68 been formally assessed using state of the art high-density mapping. The aim of this study was to relate
69 the vulnerable region delineated by RVI to the VT site of origin (VT-SoO) and compare RVI to other
70 spatio-temporal metrics of activation and repolarization.

71 **Methods**

72 **Concept and quantification of RVI**

73 The RVI concept is illustrated in Figure 1. Panel A illustrates the case of bidirectional block and no re-
74 entry: An activation wavefront (orange line) arrives at a region that is refractory and blocks (point P).
75 The wavefront travels around the area of block (orange line) and arrives back at the distal side of the
76 block (point D) which is still refractory and blocks in the reverse direction (bidirectional block).
77 Bidirectional block occurs because repolarization time at point P is longer than activation time at point
78 D. Panel B illustrates the case where re-entry occurs. The returning wavefront arrives back at the initial
79 site of block (point D) when the region proximal to it has regained excitability. The returning wavefront
80 is now able to propagate back to the proximal region and complete a re-entrant circuit. Re-entry
81 occurs because repolarization time at point P is shorter than activation time at point D. The re-entry
82 vulnerability index (RVI) is represented by the interval between activation time at the distal site D and
83 repolarization at the proximal site P, i.e. $RT_P - AT_D$, shown as shaded areas in Figure 1. A shorter RVI
84 (panel B) is more likely to be associated with re-entry than a longer RVI (panel A).

85

86 **Patients and procedures**

87 Patients with structural heart disease undergoing catheter ablation for VT were prospectively
88 recruited at the Barts Heart Centre and St Thomas's Hospital, London, UK. Patients gave informed
89 consent for inclusion into VT mapping research approved by local REC. Cardiac mapping was
90 performed either with CARTO (Pentaray and Decanav) or with EnSite Precision (HD Grid) (Table 1). The
91 mapping data were included in the study if the VT-SoO was identified and a sufficiently dense
92 substrate map was produced.

93 Mapping was performed during ventricular pacing from the RV apex. If pacing was well tolerated, a
94 train of 5 S_1 paced beats was delivered followed by an S_2 beat at a short coupling interval (Table 1) to

95 induce slow conduction necessary for RVI calculation ⁷. If continuous pacing was poorly tolerated,
96 either a train of three short coupled beats were delivered or a single paced beat was delivered shortly
97 after sensing the R-wave of a sinus beat. In one patient with severely impaired function, biventricular
98 pacing was delivered at a normal rate (60 bpm). The pacing procedure was continuously repeated and
99 data collected on the post-extra systolic beat using standard criteria to enable high-density sequential
100 mapping

101 In case of haemodynamically tolerated VTs, identification of VT-SoO was defined either by
102 entrainment or by termination of VT during ablation. For unstable VTs, the VT-SoO was identified using
103 pace mapping with an average correlation coefficient between the 12 lead ECG of VT and the paced
104 beat $\geq 90\%$ ¹¹. If multiple sites for the same VT were identified with pace mapping, the site providing
105 the highest correlation was retained.

106 Ablation was delivered at the VT sites of origin and at other sites to achieve substrate modification
107 using standard criteria ² and was not based on RVI, which was computed off-line.

108

109 **Data Analysis**

110 Unipolar electrograms were recorded with band-pass filters set at 0.05-500 Hz and were exported
111 along with anatomical data for bespoke off-line analysis in Matlab (Mathwork), which included
112 stringent criteria for selecting only beats showing very similar activation/repolarization patterns (see
113 Supplemental Methods). AT, RT and ARI were measured following standard definitions ^{12,13} (Figure 2)
114 using automatic robust algorithms developed and tested during the course of previous studies ^{10,14-17}.
115 Markers were revised using bespoke graphical user interfaces and semi-automatic correction, which
116 involved performing automatic annotation within manually adjusted windows of interest. Correction
117 was limited to isolated outliers to reduce arbitrary annotation and ensure reproducibility.

118 **Localization of sites vulnerable to re-entry**

119 The algorithm for RVI mapping operates as follow: For each cardiac site, neighbouring electrode sites
120 are identified within a searching radius $R=8$ mm. The intervals between RT at a given site P and AT at
121 neighbouring sites D, i.e. RT_P-AT_D , are measured. The shortest of these intervals represent the RVI at
122 site P. An RVI value was thereby obtained for each electrode site in the mapped area. This process is
123 summarized in Figure 3, where an example is provided.

124 For the sake of comparison, local gradients of AT, ARI and RT, which provide a quantification of local
125 activation and repolarization heterogeneity, were also computed (Figure 3).

126 The distance between the VT-SoO and the nearest of the following sites was measured in order to
127 assess the capability of localizing critical sites for VT initiation:

- 128 • Sites showing the lowest RVI, i.e. $RVI < 5^{\text{th}}$ percentile of RVI values. $RVI \geq 300$ ms were excluded
129 from those considered as vulnerable to re-entry even if within the lowest 5%.
- 130 • Sites showing the largest AT, RT and ARI gradients, i.e. sites for which local gradients were $>$
131 the 95^{th} percentile of their distributions.
- 132 • Sites showing the longest AT, i.e. $AT > 95^{\text{th}}$ percentile of AT values.
- 133 • Sites showing the longest RT and ARI, i.e. sites for which RT and ARI were $>$ the 95^{th} percentile
134 of their distributions.
- 135 • Sites showing the shortest RT and ARI, i.e. sites for which RT and ARI were $<$ the 5^{th} percentile
136 of their distributions.

137

138 **Statistical Analysis**

139 Data are reported as median, 1^{st} — 3^{rd} quartiles. The Wilcoxon signed-rank test was used for comparing
140 distances between VT-SoO and vulnerable sites identified by different markers with $P < 0.05$ indicating
141 significance.

142 **Results**

143 In total, 18 patients were included in the study. Baseline characteristics are reported in Table 1.
144 Patients were aged 65, 52—70 years (median, 1st—3rd) and 16 were male. Pathologies included
145 ischaemic heart disease (n=14, 78%) and ARVC (n=4, 22%). The cycle length of the beat preceding the
146 mapped beat was 360, 360—398 ms and electro-anatomical maps for RVI calculation included 1012,
147 408—2098 unipolar electrograms (Table 1). Some patient presented more than 1 VT morphology at
148 the time of the procedure, but in all cases the site of origin of only one VT was identified and confirmed
149 by either entrainment (n=6) or pace mapping (n=12) (Table 1). Other VTs were not mapped either
150 because they were thought not to be clinical or because a substrate ablation approach was preferred.
151 This was often the case, as VT was unstable in two third of patients.

152 Acute VT-inducibility was tested at the end of the procedure in 12 patients (67%), while considered
153 inappropriate in the other 6 (33%) owing to haemodynamic compromise. None of the mapped VTs
154 was inducible at the end of the procedure, while in 2 (16%) patients a different VT morphology was
155 induced.

156 During the follow-up (16.2, 7.1-20.3 months, median, minimum-maximum), 50% of patients (75% of
157 ARVC and 43% of ischemic patients) suffered a recurrence, defined as any therapy from the
158 implantable device, including anti-tachycardia pacing, heart transplant or death from any cause.

159

160 **Assessment of RVI in relation to VT sites of origin**

161 Figures 4A-C shows RVI maps in a patient for which the VT-SoO was identified by entrainment. The
162 sites of lowest RVI are clustered around the VT-SoO, with the closest one being 3.1 mm away from it.
163 Unipolar electrograms from electrode sites with large and low RVI are shown in Figure 4D-E. Figure
164 5A-C shows examples from another patient, where the VT-SoO was identified by pace mapping. In this
165 case, the distance between lowest RVI sites and the VT-SoO was 3.4 mm. Some of the lowest RVI sites
166 are distant from the VT-SoO, which is expected as these may be related to a different re-entrant circuit

167 from that identified during the procedure. Unipolar electrograms are shown in Figure 5D-E, with low
168 amplitude fractionated signals recorded at site of low RVI (panel E) close to the VT-SoO.

169 Considering all 18 VTs, the distance between sites of lowest RVI and the VT-SoO was 5.1, 3.2–10.1
170 mm (median, 1st – 3rd quartile) (Table 1). This was not different in ischaemic and ARVC patients (4.9,
171 3.1-10.7 mm vs 5.2, 2.6-11.6 mm, P=0.95) or in VTs whose site of origin was identified using pace
172 mapping vs entrainment (5.1, 4.1-9.5 mm vs 4.0, 2.5-17.9 mm, P=0.82).

173 Similar results were obtained using searching radius $R = \{7, 8, 9, 10\}$ mm, but for smaller search radii
174 the distance between the vulnerable region and the VT-SoO increased (Supplementary Figure 1).

175

176 **Comparison between RVI and other markers in relation to VT sites of origin**

177 The distance between the VT-SoO and lowest RVI sites was shorter than that for any other activation-
178 repolarization marker (Figure 6). Pair-wise comparisons showed that the distance to the VT-SoO was
179 significantly shorter for lowest RVI sites than for sites showing longest RT (P=0.020), longest ARI
180 (P=0.004) and shortest RT (P=0.042). Despite showing the lowest median value as well as lowest
181 standard deviation across all mapped VTs, distance to the VT-SoO from lowest RVI sites was not
182 significantly smaller than distance to the VT-SoO from sites showing largest local gradients of AT (G_{AT} ,
183 P=0.17), ARI (G_{ARI} , P=0.49), RT (G_{RT} , P=0.11), or from sites showing lowest ARI (0.68) and largest AT
184 (P=0.13) (Figure 6).

185 The identification of VT-SoO was considered accurate if the distance to the VT-SoO was <10 mm and
186 inaccurate if >20 mm. RVI showed the highest accuracy, with 13 VT-SoO out of 18 located within 10
187 mm to lowest RVI sites (72.2%, Figure 7A) as well as the lowest inaccuracy rate, with only 1 VT-SoO
188 located at more than 20 mm from lowest RVI sites (5.6%, Figure 7B). Inaccurate identification of VT-
189 SoO was significantly less likely to occur for lowest RVI than for longest AT and longest ARI (odd ratio
190 equal to 0.12, P=0.035, Chi-squared test, for both markers, Figure 7B).

191 **Interaction between RVI and other markers**

192 RVI showed positive correlation with ARI, $cc = 0.71, 0.59\text{--}0.76$, and RT, $cc = 0.52, 0.23\text{--}0.72$, and a
193 weaker inverse correlation with AT, $cc = -0.26, -0.45\text{--}-0.07$, G_{AT} , $cc = -0.25, -0.47\text{--}-0.12$ and G_{ARI} , cc
194 $= -0.26, -0.44\text{--}0.09$ (Supplementary Figure 2A).

195 Sites with lowest RVI partially overlapped with those showing shortest RT and ARI, with overlap equal
196 to 35%, 23—42% and 24%, 12—44%, respectively (Supplementary Figure 2B). Only 5%, 0%—16% of
197 sites with lowest RVI were also identified as vulnerable owing to longest AT. This increased to 13%,
198 0%—21% when considering as overlapping sites situated at a distance ≤ 2 mm. About 15% of sites
199 showing lowest RVI also showed largest gradients of AT or ARI. This suggests that RVI captures
200 electrophysiological vulnerability independently from standard activation-repolarization markers.

201

202 **Discussion**

203 This is the first study to use state of the art mapping technology to comprehensively evaluate the RVI
204 and alternative activation-repolarization markers in delineating the sites critical for VT establishment.

205 The main results are: (1) RVI identifies vulnerable regions that were within 10 mm of VT-SO in 72.2%
206 of VTs and >20 mm away in only 5.6% of VTs, with the closest vulnerable site located 5.1, 3.2—10.1
207 mm from the VT-SoO. (2) Inaccurate VT-SoO identification was significantly less frequent for lowest
208 RVI than for longest AT and longest ARI. (3) Lowest RVI identifies vulnerable regions independent of
209 other activation and repolarization markers and it incorporates information from both local AT and
210 ARI gradients, which identified critical regions at a (non-significantly) larger distance than lowest RVI.

211 RVI is based upon a conceptual model of the critical relationship between activation and repolarization
212 restitution properties, which was formerly defined by Coronel and colleagues in an elegant animal
213 study⁶. That study demonstrated that the critical parameter to differentiate block from the initiation
214 of re-entrant arrhythmia was the interval between the proximal RT of the premature beat and the

215 arrival time of the premature wave at the distal side of the line of block. This represents the foundation
216 of the RVI algorithm, first implemented by Taggart and colleagues in a mechanistic proof-of-principle
217 study ⁷. Results from retrospective analysis of non-contact mapping data in selective RV disorders ¹⁰
218 and computational studies ^{8,9} have provided support to the validity of the RVI concept. This study has
219 assessed for the first time the RVI as a potential clinical tool to identify critical targets for ablation by
220 utilising state of the art mapping technology in both RV and LV pathologies and comparing it to other
221 activation-repolarization metrics of functional substrate. The results suggest that RVI could represent
222 a useful metric to inform novel substrate ablation strategies.

223 While other studies have focused on improving the delineation of the arrhythmogenic substrate with
224 late potentials ^{18,19}, metrics related to slow conduction, visualization of potential diastolic pathway
225 and characterization of channels using imaging ^{2,20}, this study demonstrates that repolarization is
226 critical for the identification of VT-SoO.

227 RVI performed similarly to, but independently of, local gradients of activation, an established marker
228 of arrhythmia susceptibility ²¹, which is embedded in the RVI concept. A moderate correlation between
229 RVI and local activation and repolarization gradients confirms the theoretical observation that RVI
230 integrates information from both activation and repolarization dynamics.

231 **Current performance and future developments**

232 Despite its solid theoretical underpinning, RVI was not significantly superior to other markers in the
233 identification of the VT-SoO. This may be partially due to lack of statistical power (n=18) and both
234 procedural and technological limitations. A critical aspect of RVI is the pacing protocol, with both cycle
235 length and pacing site potentially affecting RVI maps ⁸. The importance of stimulating the tissue at a
236 coupling interval short enough to engage conduction velocity restitution to unmask
237 electrophysiological vulnerability is well recognised ¹⁹. It may be possible that a more aggressive S₁S₂
238 pacing protocol could have provided more precise localisation but at the risk of haemodynamic
239 compromise and VT induction in these vulnerable patients. The pacing site affects both voltage ²² and

240 activation-repolarization properties ²³ and pacing from multiple sites may improve RVI delineation of
241 the arrhythmogenic substrate ⁸. This was not feasible due to time constraints during the procedure.

242 Importantly, in structurally abnormal hearts, multiple pathways may support different VTs, some of
243 which may not be revealed during the procedure. This limits the extent by which any metric
244 theoretically related to sites susceptible to re-entry can be validated using information from the VTs
245 mapped during the procedure. Validation by prospective studies using ablation to target all low RVI
246 sites will be required in randomised controlled trials to test this physiological mapping approach
247 versus current VT ablation strategies to determine VT recurrence, hospitalisations and mortality.

248 **Limitations**

249 Although bespoke software solutions were implemented to analyse only beats with the same
250 activation-repolarization sequence and semi-automatic correction was kept to a minimum to ensure
251 reproducibility, repolarization variability during sequential mapping and the challenge of measuring
252 activation/repolarization markers in diseased myocardium may have affected the results. Ultra-fast
253 non-contact mapping providing AT and RT within one single beat may represent a possible solution ²⁴.

254 The identification of VT-SoO with pacing manoeuvres presents limitations inherent to electro-
255 anatomical mapping. Pace-mapping is a standard approach to identify the exit site of unstable VTs ¹¹,
256 but its accuracy can be affected by area of capture and functional block only present in VT. A previous
257 study has reported 82% sensitivity and 87% specificity in identifying the exit region by pace mapping
258 with a 82% morphology match ¹¹. Our cut-off value of 90% morphology match should provide slightly
259 higher specificity. Although none of the mapped VTs were inducible after ablation, acute VT induction
260 could not be consistently tested as procedural end-point owing to hemodynamic compromise in 6
261 patients. The recurrence rate was 50% after a median follow-up of 16 months, which is in line with
262 other studies ¹. This is likely due to limitations of current ablation strategies in complex patients with
263 haemodynamic compromise and presenting multiple potential vulnerable sites for VT development
264 most of which are concealed at the time of the procedure and cannot be localized with entrainment,

265 pace-mapping or standard substrate mapping. This study did not set out to prospectively ablate low
266 RVI sites, which will be the subject of future studies to assess whether this influences outcomes.

267 **Conclusions**

268 These data show that RVI identifies vulnerable regions that closely correlate with the VT site of origin
269 and suggest that activation-repolarization metrics may improve the delineation of the arrhythmogenic
270 substrate and enable optimal substrate based ablation without the risks of compromising the patient
271 with multiple VT inductions.

272

273 **Acknowledgements**

274 FOC, MJB and BMH acknowledge the support of the British Heart Foundation through Project Grant
275 PG/16/81/32441. PDL is supported by UCLH Biomedicine NIHR and Barts BRC, Stephen Lyness
276 Research Fund.

277 **References**

- 278 1. Shivkumar K: Catheter Ablation of Ventricular Arrhythmias. Jarcho JA, ed: N Engl J Med
279 Massachusetts Medical Society, 2019; 380:1555–1564.
- 280 2. Santangeli P, Marchlinski FE: Substrate mapping for unstable ventricular tachycardia. Heart
281 Rhythm Elsevier, 2016; 13:569–583.
- 282 3. Bourier F, Martin R, Martin CA, et al.: Is it feasible to offer “targeted ablation” of ventricular
283 tachycardia circuits with better understanding of isthmus anatomy and conduction
284 characteristics? Europace Narnia, 2019; 21:I27–I33.
- 285 4. Josephson ME, Anter E: Substrate Mapping for Ventricular Tachycardia. JACC Clin
286 Electrophysiol 2015; 1:341–352.

- 287 5. Mines GR: On dynamic equilibrium in the heart. *J Physiol Wiley-Blackwell*, 1913; 46:349–383.
- 288 6. Coronel R, Wilms-Schopman FJG, Opthof T, Janse MJ: Dispersion of repolarization and
289 arrhythmogenesis. *Heart Rhythm* 2009; 6:537–543.
- 290 7. Child N, Bishop MJ, Hanson B, et al.: An activation-repolarization time metric to predict
291 localized regions of high susceptibility to reentry. *Heart Rhythm* 2015; 12:1644–1653.
- 292 8. Hill YR, Child N, Hanson B, Wallman M, Coronel R, Plank G, Rinaldi CA, Gill J, Smith NP, Taggart
293 P, Bishop MJ: Investigating a novel activation-repolarisation time metric to predict localised
294 vulnerability to reentry using computational modelling. *PLoS One Public Library of Science*,
295 2016; 11:e0149342.
- 296 9. Campos FO, Orini M, Taggart P, Hanson B, Lambiase PD, Porter B, Rinaldi CA, Gill J, Bishop MJ:
297 Characterizing the clinical implementation of a novel activation-repolarization metric to
298 identify targets for catheter ablation of ventricular tachycardias using computational models.
299 *Comput Biol Med Pergamon*, 2019; 108:263–275.
- 300 10. Martin CA, Orini M, Srinivasan NT, Bhar-Amato J, Honarbakhsh S, Chow AW, Lowe MD, Ben-
301 Simon R, Elliott PM, Taggart P, Lambiase PD: Assessment of a conduction-repolarisation metric
302 to predict Arrhythmogenesis in right ventricular disorders. *Int J Cardiol* 2018; 271:75–80.
- 303 11. De Chillou C, Groben L, Magnin-Poull I, et al.: Localizing the critical isthmus of postinfarct
304 ventricular tachycardia: The value of pace-mapping during sinus rhythm. *Heart Rhythm*
305 Elsevier, 2014; 11:175–181.
- 306 12. Coronel R, de Bakker JMT, Wilms-Schopman FJG, Opthof T, Linnenbank AC, Belterman CN,
307 Janse MJ: Monophasic action potentials and activation recovery intervals as measures of
308 ventricular action potential duration: Experimental evidence to resolve some controversies.
309 *Heart Rhythm* 2006; 3:1043–1050.
- 310 13. Orini M, Srinivasan NT, Graham A, Taggart P, Lambiase P: Further evidence on how to measure

- 311 local repolarization time using intracardiac unipolar electrograms in the intact human heart.
312 *Circ Arrhythm Electrophysiol* 2019; .
- 313 14. Orini M, Taggart P, Lambiase PD: In vivo human sock-mapping validation of a simple model that
314 explains unipolar electrogram morphology in relation to conduction-repolarization dynamics.
315 *J Cardiovasc Electrophysiol* 2018; 29:990–997.
- 316 15. Orini M, Taggart P, Srinivasan N, Hayward M, Lambiase PD: Interactions between activation
317 and repolarization restitution properties in the intact human heart: In-vivo whole-heart data
318 and mathematical description. *PLoS One* 2016; 11:e0161765.
- 319 16. Orini M, Yanni J, Taggart P, et al.: Mechanistic insights from targeted molecular profiling of
320 repolarization alternans in the intact human heart. *Europace* 2019; 21:981–989.
- 321 17. Orini M, Citi L, Hanson BMBM, Taggart P, Lambiase PDPDPD: Characterization of the causal
322 interactions between depolarization and repolarization temporal changes in unipolar
323 electrograms. *Computing in Cardiology IEEE*, 2013, pp. 719–722.
- 324 18. Vergara P, Trevisi N, Ricco A, Petracca F, Baratto F, Cireddu M, Bisceglia C, Maccabelli G, Della
325 Bella P: Late potentials abolition as an additional technique for reduction of arrhythmia
326 recurrence in scar related ventricular tachycardia ablation. *J Cardiovasc Electrophysiol* John
327 Wiley & Sons, Ltd (10.1111), 2012; 23:621–627.
- 328 19. Porta-Sánchez A, Jackson N, Lukac P, et al.: Multicenter Study of Ischemic Ventricular
329 Tachycardia Ablation With Decrement-Evoked Potential (DEEP) Mapping With Extra Stimulus.
330 *JACC Clin Electrophysiol Elsevier*, 2018; 4:307–315.
- 331 20. Sramko M, Hoogendoorn JC, Glashan CA, Zeppenfeld K: Advancement in cardiac imaging for
332 treatment of ventricular arrhythmias in structural heart disease. *Europace* 2019; 21:383–403.
- 333 21. Ciaccio EJ, Chow AW, Davies DW, Wit AL, Peters NS: Localization of the Isthmus in Reentrant
334 Circuits by Analysis of Electrograms Derived from Clinical Noncontact Mapping during Sinus

335 Rhythm and Ventricular Tachycardia. J Cardiovasc Electrophysiol John Wiley & Sons, Ltd
336 (10.1111), 2004; 15:27–36.

337 22. Tung R, Josephson ME, Bradfield JS, Shivkumar K: Directional Influences of Ventricular
338 Activation on Myocardial Scar Characterization: Voltage Mapping with Multiple Wavefronts
339 during Ventricular Tachycardia Ablation. Circ Arrhythmia Electrophysiol 2016; 9.

340 23. Srinivasan NT, Orini M, Simon RB, et al.: Ventricular stimulus site influences dynamic dispersion
341 of repolarization in the intact human heart. Am J Physiol - Hear Circ Physiol 2016; 311:H545–
342 H554.

343 24. Graham AJ, Orini M, Zacur E, et al.: Simultaneous Comparison of Electrocardiographic Imaging
344 and Epicardial Contact Mapping in Structural Heart Disease. Circ Arrhythm Electrophysiol 2019;
345 12:e007120.

346

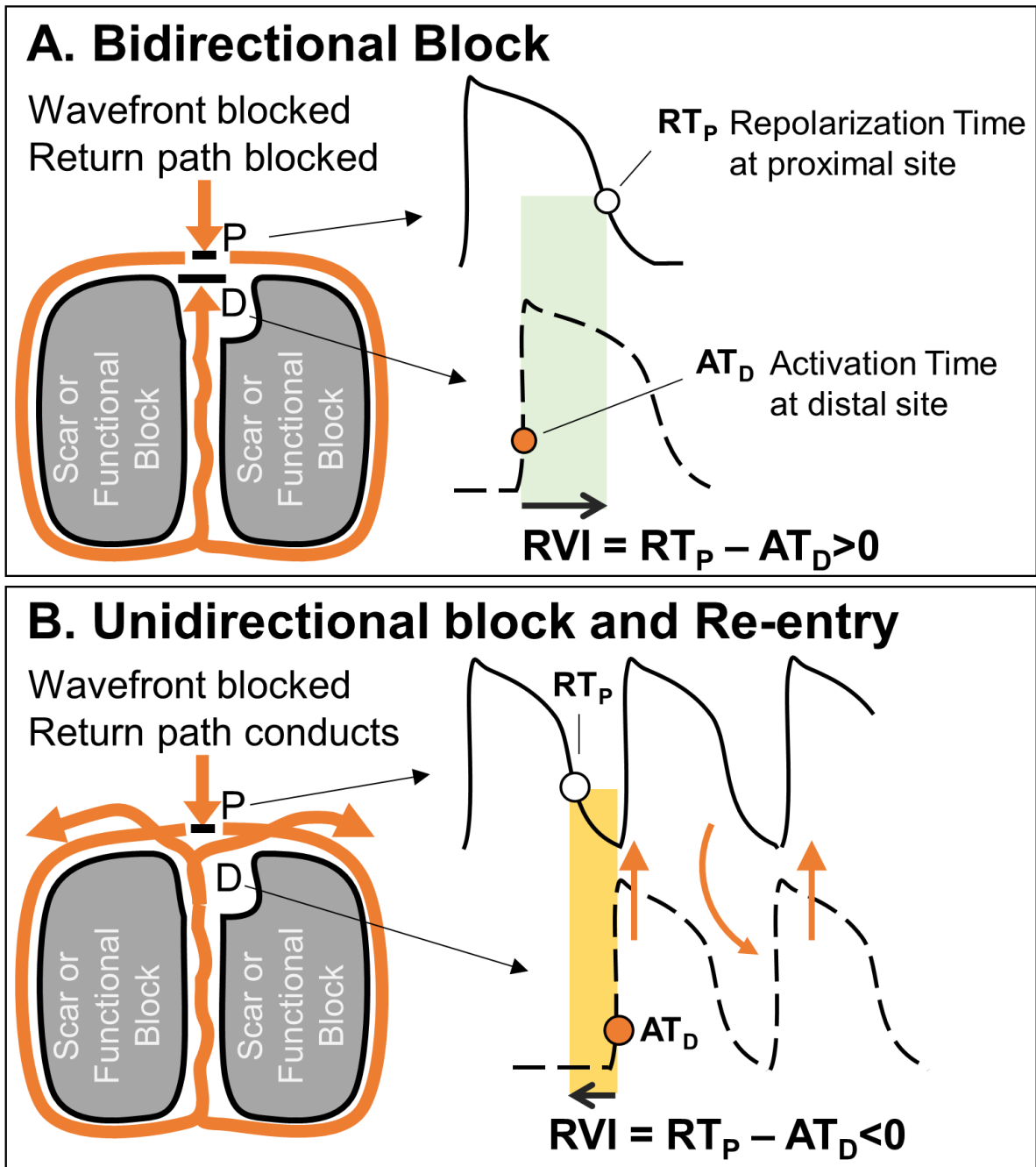
347

348 **Tables**

	Sex	Age (years)	Aetiology	VT-SoO	EAM	Catheter	Pacing Interval (ms)	Pacing Type	Points on Map (n)	Dist to VT-SoO (mm)
1	M	69	IHD	PM	CARTO	Pentaray	500	S1S1	4190	8.3
2	F	34	ARVC	ENT	CARTO	Pentaray	460	S1S1	2256	17.9
3	M	71	IHD	PM	CARTO	Pentaray	360	S1S2	2560	4.9
4	F	52	ARVC	PM	CARTO	Pentaray	360	S1S1	1312	5.2
5	M	79	IHD	ENT	CARTO	Pentaray	380	S1S2	260	4.8
6	M	55	IHD	PM	CARTO	Pentaray	360	S1S2	1625	8.2
7	M	70	IHD	PM	CARTO	Pentaray	360	S1S2	370	16.5
8	M	73	ARVC	PM	CARTO	Pentaray	360	S1S2	328	5.2
9	M	22	ARVC	PM	CARTO	Decanav	1000	S1S1 ^{BV}	4325	0.0
10	M	65	IHD	ENT	Precision	HD-Grid	360	SE	1341	33.9
11	M	68	IHD	PM	Precision	HD-Grid	360	SE	1304	13.8
12	M	50	IHD	PM	Precision	HD-Grid	360	SE	4328	10.7
13	M	61	IHD	ENT	Precision	HD-Grid	325	SE	719	1.9
14	M	65	IHD	PM	Precision	HD-Grid	360	S1S2	356	3.4
15	M	77	IHD	PM	Precision	HD-Grid	400	SE	389	5.0
16	M	60	IHD	PM	Precision	HD-Grid	390	SE	466	1.7
17	M	52	IHD	ENT	Precision	HD-Grid	360	SE	511	3.1
18	M	65	IHD	ENT	Precision	HD-Grid	400	SE	667	2.5
	89% M	65 (53-70)	72% IHD	67% PM	50% CARTO	HD-Grid 50%	360 (360-398)	44% SE	1012 (408-2098)	5.1 (3.2-10.1)

349

350 **Table 1:** Patient's information. IHD: ischemic heart disease; ARVC: Arrhythmogenic Right Ventricular
351 Cardiomyopathy. Pacing manoeuvres to determine the VT site of origin, VT-SoO, were either
352 entrainment (ENT) or pace mapping (PM). Electro-anatomical mapping systems were CARTO or Ensite
353 Precision. Pacing types were S1S1, S1S2 or sensed-extras (SE). S1S1^{BV} denotes bi-ventricular pacing.
354 Points on Map is the number of unipolar electrograms per map. Dist to VT-SoO is the distance between
355 the VT site of origin and the nearest site showing lowest RVI.



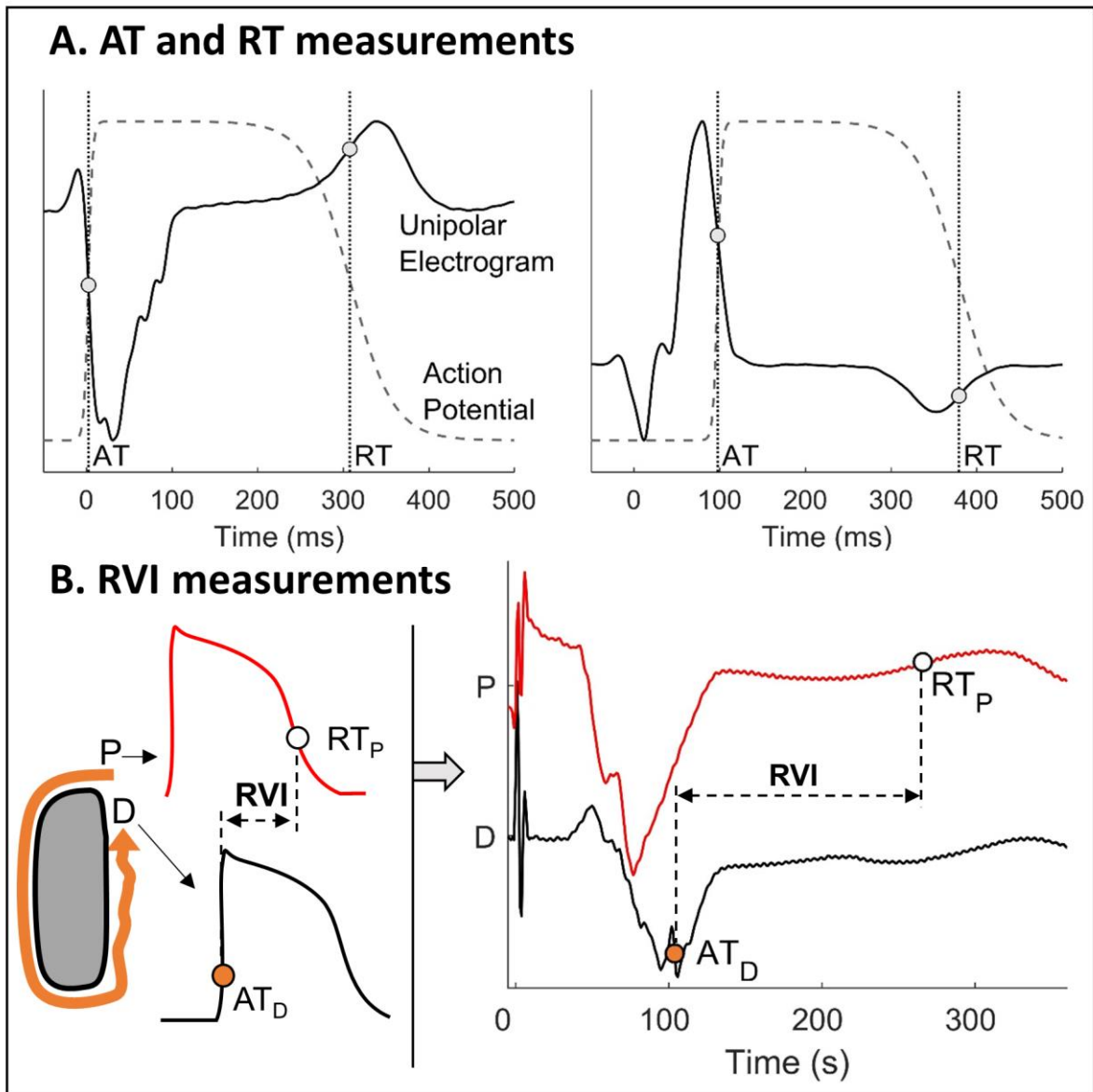
357

358 **Figure 1:** Theoretical model underpinning the re-entry vulnerability index (RVI). See text. Similar

359 diagrams can be found in ^{6,7,10}.

360

361



362

363 **Figure 2: Computation of spatial activation-repolarization metrics.** A: Stylised action

364 potentials and unipolar electrograms showing standard measurements of activation (AT) and

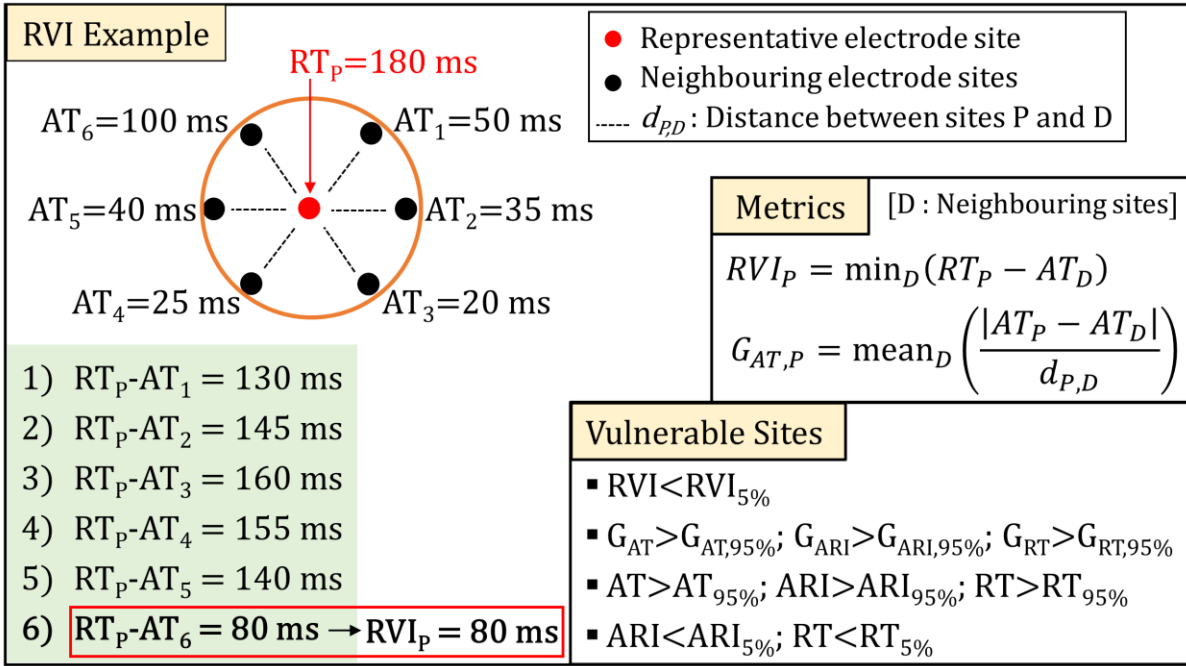
365 repolarization (RT) times. B: Conceptual model for RVI measurement (left) and RVI

366 measurements using recorded unipolar electrograms (right).

367

368

369

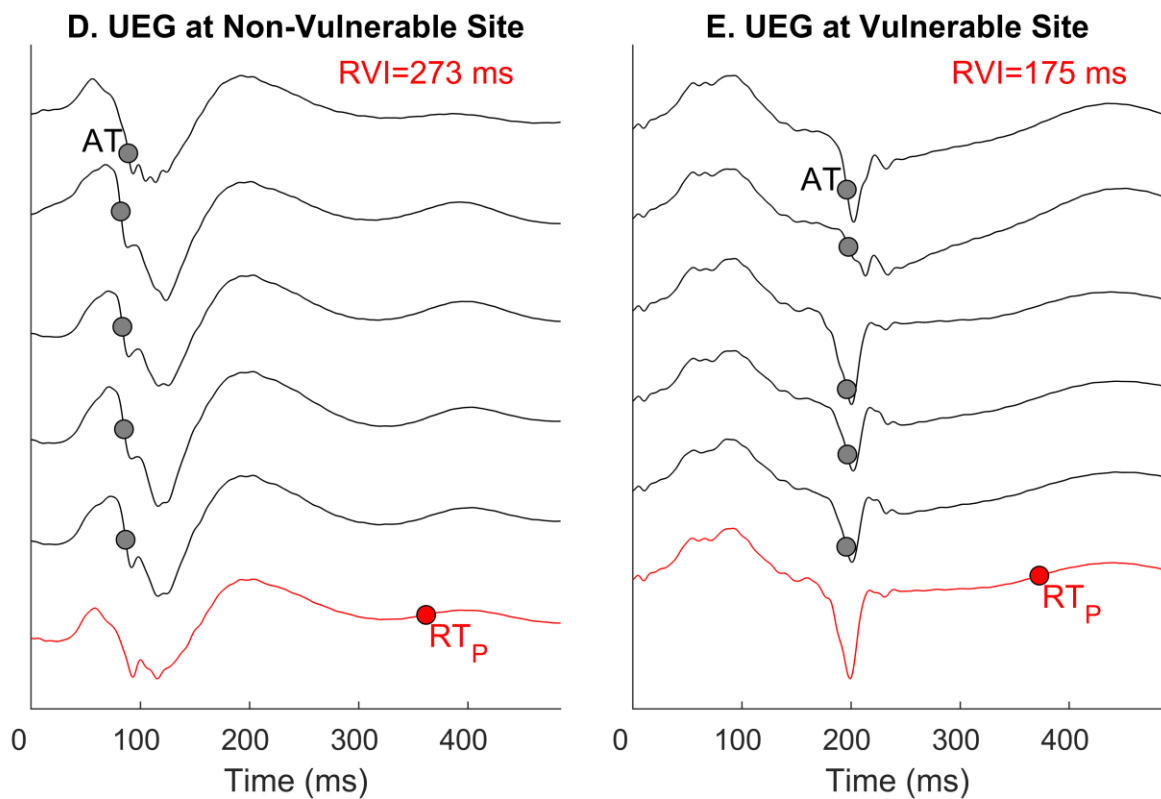
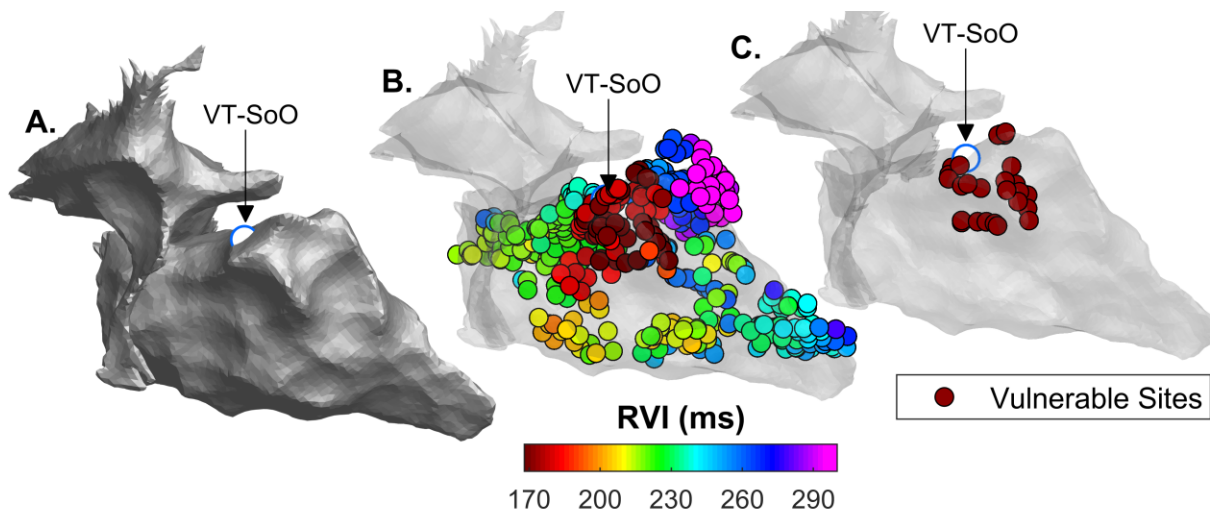


370

371 **Figure 3: Computation of RVI and spatial activation-repolarization metrics.** Left: The red dot
 372 represents a cardiac site P for which RVI is measured. Black dots represent neighbouring cardiac sites
 373 within a searching radius R. As shown in the example in the box, RVI is the shortest interval between
 374 AT at neighbouring sites and RT at site P, $RT_P - AT_D$. The formula for RVI and local gradients
 375 measurement are reported on the right. Local gradients of ARI and RT are measured in the same way.
 376 The criteria for identifying vulnerable sites to re-entry are given in the bottom-right panel.

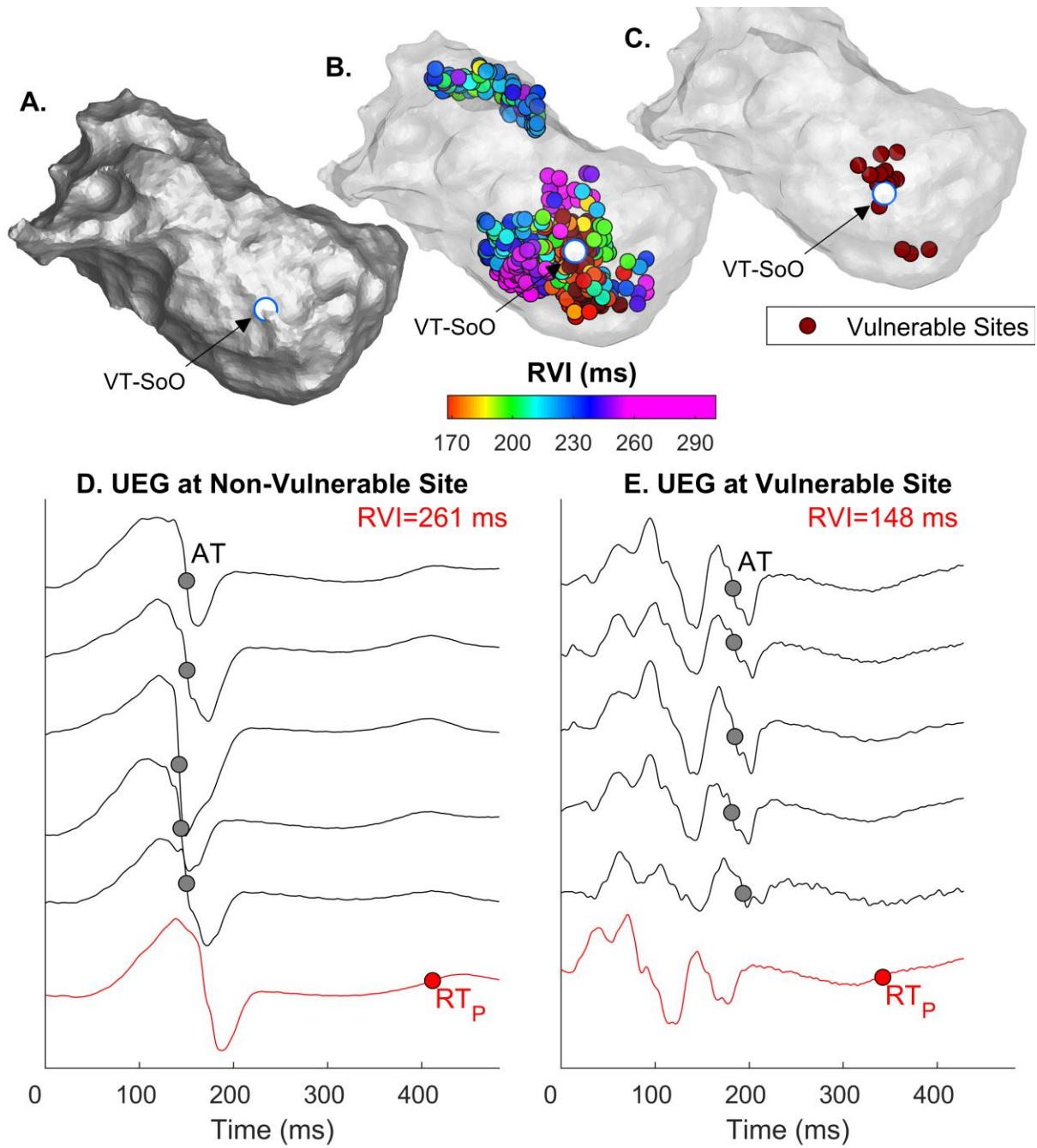
377

378



379

380 **Figure 4: Example of RVI identifying vulnerable sites close to an entrained VT.** A: Anatomical map
 381 showing the VT site of origin (VT-SoO) as a white dot. B: RVI map where each dot represents a cardiac
 382 site and RVI is colour-coded. C: map showing sites showing the lowest 5% of RVI values. D-E: Unipolar
 383 electrograms from an electrode site showing high (D) and low (E) RVI (red line) and from neighbouring
 384 electrode sites (grey). Red and grey circles represent RT at the site of RVI measurement, RT_p , and AT
 385 at neighbouring sites, respectively.



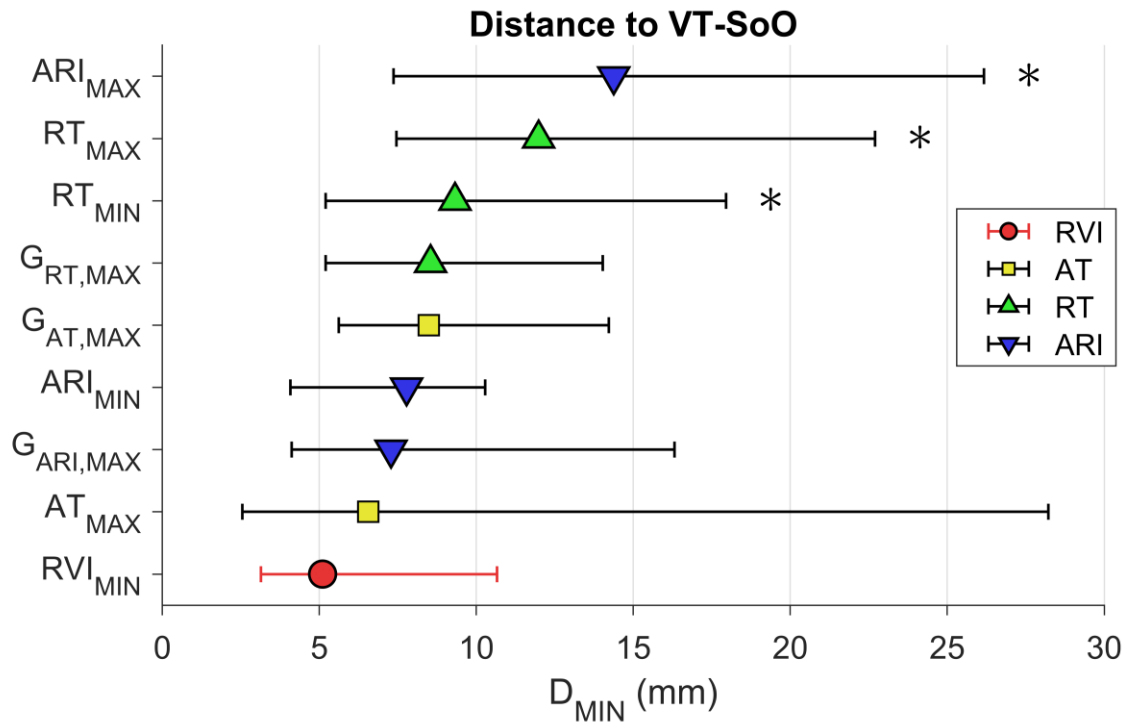
387

388 **Figure 5: Example of RVI identifying vulnerable sites close to a pace-mapped VT. See Figure 4's**

389 legend for details.

390

391

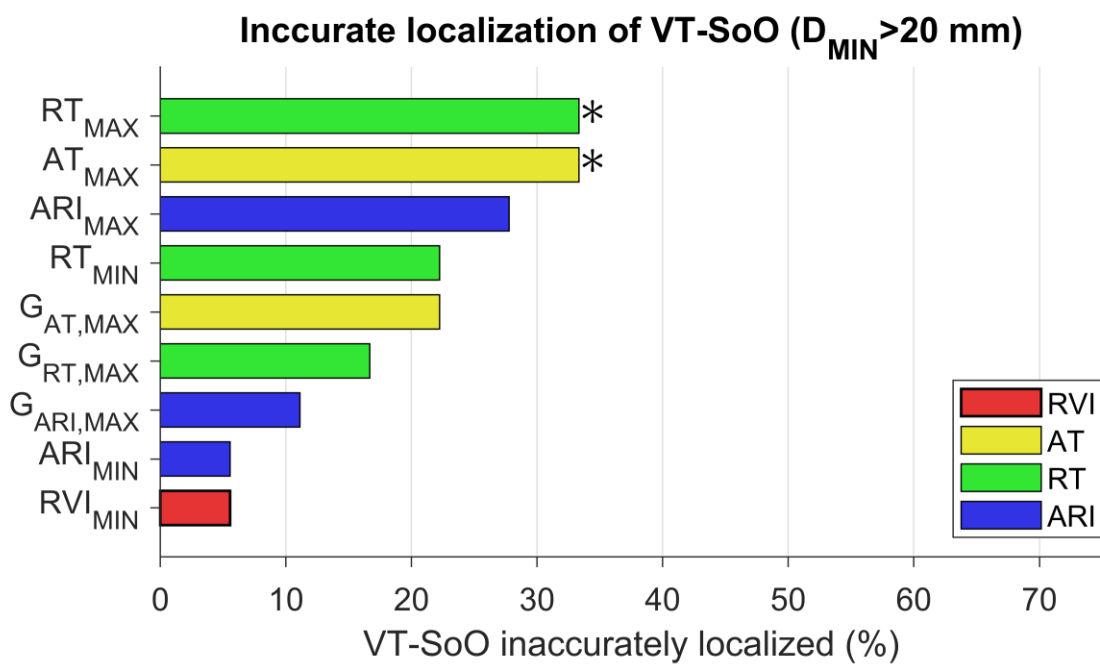
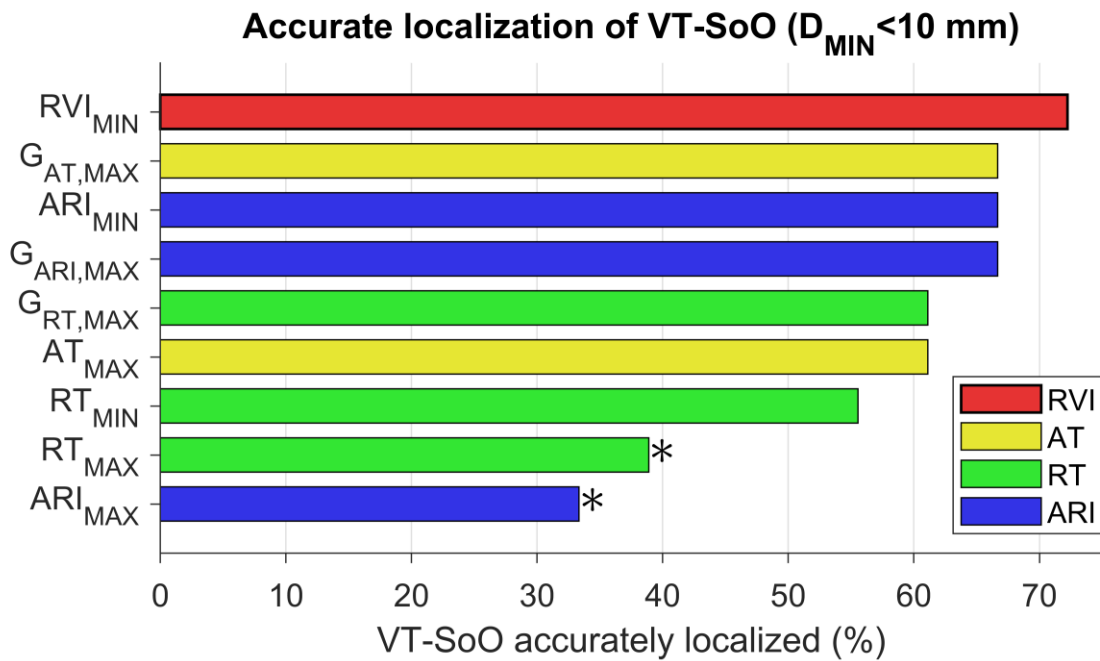


392

393 **Figure 6: Distance to VT site of origin.** Distance between the VT site of origin (VT-SoO) and nearest
 394 vulnerable sites identified by lowest RVI (RVI_{MIN}), largest gradients of AT ($G_{AT,MAX}$), largest gradients of
 395 RT ($G_{RT,MAX}$), largest gradients of ARI ($G_{ARI,MAX}$), longest AT (AT_{MAX}), shortest RT (RT_{MIN}), longest RT
 396 (RT_{MAX}), shortest ARI (ARI_{MIN}) and longest ARI (ARI_{MAX}). Markers indicate the median of minimum
 397 distances and bars span the 1st–3rd quartile interval (across n=18 VTs). *: $P < 0.05$ with respect to
 398 RVI_{MIN} .

399

400



401

402 **Figure 7: Accuracy of VT sites of origin localization.** Proportion of VTs for which the distance between

403 VT-SoO and the vulnerable sites was < 10 mm (A, accurate localization of VT-SoO). > 20 mm (B,

404 inaccurate localization of VT-SoO). * : $P < 0.05$ with respect to RVI_{MIN}.

405